Revista Mexicana de Física
ISSN: 0035-001X
rmf@ciencias.unam.mx
Sociedad Mexicana de Física A.C.
México

Aguilera, E.F.; Martinez-Quiroz, E.; Rosales, P.; Lizcano, D.; Gómez-Camacho, A.; Kolata, J.J.; Lamm, L.O.; Guimares, V.; Lichtenthäler, R.; Camargo, O.; Becchetti, F.D.; Jiang, H.; DeYoung, P.A.; Mears, P.J.; Belyaeva, T.L.
Proton-halo effects in the 8 B+ 58 Ni reaction near the Coulomb barrier
Revista Mexicana de Física, vol. 55, núm. 2, 2009, pp. 1-5
Sociedad Mexicana de Física A.C.
Distrito Federal, México

Proton-halo effects in the ^{8}B+^{58}Ni reaction near the Coulomb barrier

E.F. Aguilera, E. Martinez-Quiroz, P. Rosales, D. Lizcano, and A. Gómez-Camacho
Departamento de Aceleradores, Instituto Nacional de Investigadores Nucleares,
Apartado Postal 18-1027, 11801, México, D.F., México.

J.J. Kolata and L.O. Lamm
Physics Department, University of Notre Dame,
Notre Dame, 46556-5670 Indiana.

V. Guimarães, R. Lichtenthäler, and O. Camargo
Instituto de Fisica, Universidade de Sao Paulo,
P.O. Box 66318, 05389-970 Sao Paulo, SP, Brazil.

F.D. Becchetti and H. Jiang
Physics Department, University of Michigan,
Ann Arbor, 48109-1120 Michigan.

P.A. DeYoung and P.J. Mears
Physics Department, Hope College,
Holland, 49422-9000 Michigan.

T.L. Belyaeva
Universidad Autónoma del Estado de México,
50000, Toluca, México.

Recibido el 12 de mayo de 2009; aceptado el 6 de agosto de 2009

Elastic scattering of ^{8}B and ^{7}Be on a ^{58}Ni target has been measured at energies near the Coulomb barrier. The total reaction cross sections were deduced from Optical-model fits to the experimental angular distributions. Comparison with other systems shows evidence for proton-halo effects on ^{8}B, as well as for neutron-halo on ^{6}He reactions. While the enhancement in the cross section observed for ^{8}B is explained in terms of projectile breakup, in the case of ^{6}He reactions, the particle transfer proces explains the observed enhancement.

Keywords: Proton halo; neutron halo; elastic scattering; optical model; total reaction cross sections.

Se midió la Dispersión Elástica de ^{8}B y ^{7}Be en un blanco de ^{58}Ni a energías cercanas a la barrera Coulombiana. Las secciones totales de reacción se dedujeron de los ajustes hechos con el Modelo Óptico a las distribuciones angulares experimentales. La comparación con otros sistemas muestra evidencias de los efectos del halo protónico en el ^{8}B , así como del halo neutrónico en el ^{6}He. El acrecentamiento en las secciones observado para el ^{8}B se explica en términos del rompimiento del proyectil, mientras en el caso de las reacciones con ^{6}He, el proceso de transferencia de partículas explica el acrecentamiento.

Descriptores: Halo protónico; halo neutrónico; dispersión elástica; modelo óptico; secciones totales de reacción.

PACS: 25.60.Bx; 25.60.Dx; 25.70.-z

The short-lived radioactive nucleus ^{8}B is adjacent to the proton drip line and has a very small proton separation energy of only 0.138 MeV. The possibility of proton-halo nature of this nucleus has attracted much attention in the last decade [1–3]. Measurements of several reaction channels at energies much above the Coulomb barrier [4–10] have indicated an extended spatial distribution for the loosely bound proton in ^{8}B, but the question of the existence of a proton halo has remained open [11, 12]. More recently [13, 14], an angular distribution for ^{8}Be coming from breakup of ^{8}B on a ^{58}Ni target measured at a near-barrier energy indicates that Coulomb-nuclear interference at very large distances plays an important role. This fact reinforces the idea of the exotic proton-halo nature of this nucleus. Calculations treating the projectile as a weakly bound proton orbiting a ^{7}Be core reproduce the data quite well as long as continuum-continuum couplings are included [13, 15–17]. Single-angle measurements at energies near the Coulomb barrier gave consistent values for the absolute cross sections in agreement with the predicted trend [18]. Additional evidence for the proton halo of ^{8}B, both theoretical and experimental, has appeared in the literature in recent years [19–26].

While much work has been done on neutron-halo nuclei [27, 28], the present knowledge of proton-halo effects is rather scarce [29]. Fusion cross section and break up of projectile measurements for ^{17}F+^{208}Pb [30, 31] were made to study the proton-halo effects for this system, but it is not clear that either of these experiments gives relevant information on the effect of the proton-halo state, which is an excited state in ^{17}F. Similar considerations apply also to recent measurements for proton-rich isotopes of phosphorus [32]. As a result, it is far from clear that enhanced cross sections should be expected in the proton-halo case and it is therefore important that reaction yields near the barrier be studied for true proton-halo systems.

On the other hand, it would be desirable that at energies around the Coulomb barrier, the reaction yields for ^{8}B+^{58}Ni would show similarities with *e.g.* previous observations for the neutron-halo projectile ^{6}He, where large enhancements are observed below the barrier with a ^{209}Bi target [33–35], and also for targets closer to ^{58}Ni [36, 37].

In this work we present the preliminary results of elastic scattering measurements for ^{8}B and also its core, the radioactive nucleus ^{7}Be. Comparison with previous reported data [33–35], for the neutron-halo projectile ^{6}He also is made. A more complete analysis for ^{8}B have been recently reported [38].

Due to the method of production of secondary beams with the TwinSol facility at the University of Notre Dame [39], it is possible to obtain more than one beam simultaneously. In our case a primary beam of ^{6}Li at energies of 29, 31, 33, 35 and 37 MeV was incident on a ^{3}He gas-cell production target to obtain ^{8}B and ^{7}Be secondary radioactive beams with lab energies at the target center 20.7, 23.4, 25.3, 27.2 and 29.3 MeV for ^{8}B; and 15.1, 17.1, 18.5, 19.9 and 21.4 MeV for ^{7}Be. The typical primary beam current was 250 particle nA, giving typical secondary beam rates for ^{8}B and ^{7}Be of 4.0×10^4 and 7.3×10^4 particles/s, respectively. The corresponding energy widths (FWHM) were 0.86 and 1.11 MeV. An enriched ^{58}Ni target with a thickness of $\sim$1 mg/cm^2 was used for all energies.

The scattered particles were detected with four 24x24 mm Si position-sensitive detectors (PSDs) and one E-ΔE silicon-detector telescope. The detectors were moved to cover the angular interval between 20 and 160°. When used at small forward angles, where good statistics are obtained, the PSDs were software sectioned into two halves in order to obtain data at additional angles. A typical two dimensional spectrum obtained with E-ΔE telescope is presented in Fig. 1. The elastic groups are clearly separated in this spectrum and the data confirms that contamination from other ions was negligible. The intense ^{6}Li-group is the transmitted and scattered primary beam.

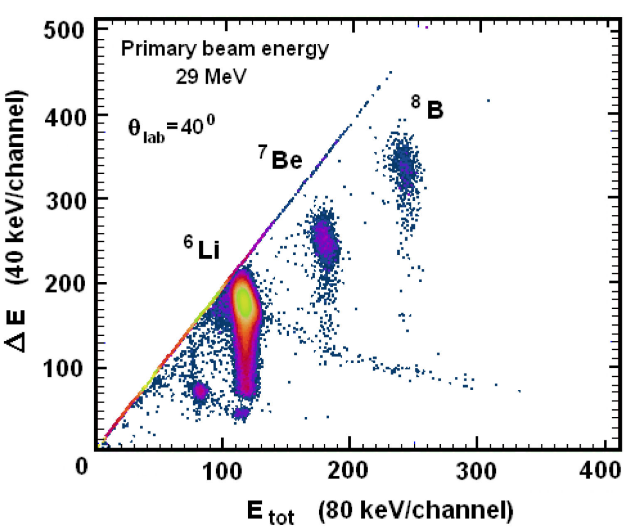

FIGURE 1. Two-dimensional spectrum obtained with E-ΔE telescope. The elastic scattering groups for ^{8}B, ^{7}Be, and ^{6}Li are indicated.

The energy resolution was sufficient to separate the ^{58}Ni first excited state (2^+, 1.45 MeV), which we did not see for any projectile. For ^{8}B, which have no bound excited states, the data are then purely elastic. On the other hand, ^{7}Be has a low-lying bound state at 0.43 MeV that cannot be resolved, so any corresponding inelastic yield is included in the data. However, for the mirror nucleus ^{7}Li, which has a similar low-energy excited state, reported measurements [40] show that the corresponding inelastic contribution is negligibly small, so this contribution will be ignored in the analysis for ^{7}Be projectile.

The obtained experimental angular distributions for the (^{8}B,^{7}Be)+^{58}Ni, are shown in the Fig. 2, upper and lower parts, respectively. For ^{8}B+^{58}Ni, the best optical-model description of the data was obtained with real and imaginary potentials of the Woods-Saxon type adjusted for each bombarding energy. The corresponding potential parameters are indicated in Table I and the results of fits are represented

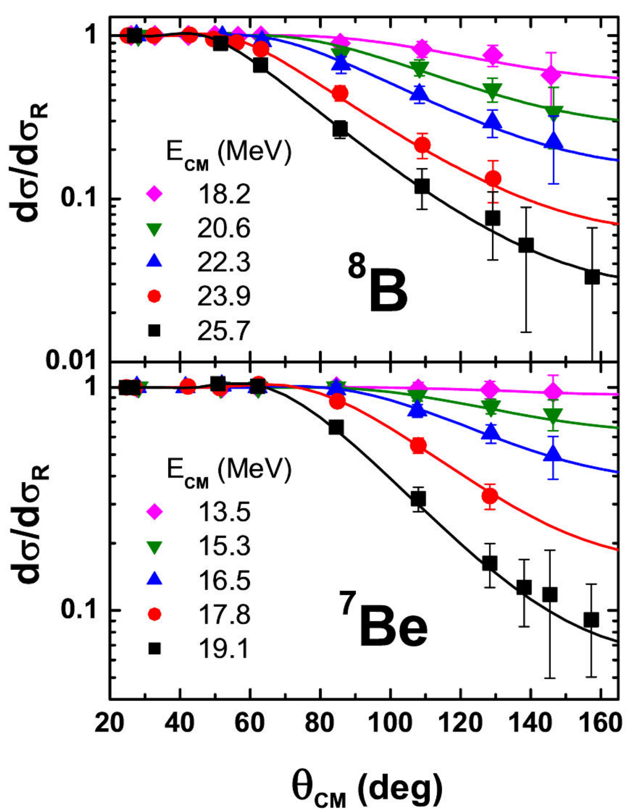

FIGURE 2. Elastic scattering angular distributions for (^{8}B,^{7}Be)+^{58}Ni at the five energies indicated. If not shown, error bars (purely statistical) are smaller than the size of the symbol. The curves correspond to optical model calculations with parameters obtained from fit, Tables I and II.

TABLE I. Optical-model potentials obtained for ^{8}B+^{58}Ni and the corresponding calculated reaction cross sections. The real and imaginary parts are volume Woods-Saxon type with radii given by $R_x = r_x \times (A_p^{1/3} + A_t^{1/3})$. The depth is in MeV and the radius and diffuseness are in fm. The Coulomb radius is r_C = 1.2 fm.

E_{lab}	V	r_R	a_R	W_V	r_I	a_I	χ^2/N	σ_R (mb)
20.7	10.0	1.30	0.56	166.9	1.26	0.65	0.15	198±50
23.4	11.8	1.30	0.53	166.8	1.22	0.61	0.58	363±50
25.3	11.9	1.28	0.54	166.8	1.21	0.60	0.33	512±50
27.2	10.8	1.30	0.53	166.9	1.24	0.62	0.41	812±45
29.3	10.0	1.30	0.52	173.8	1.26	0.61	0.13	1005±40

TABLE II. Optical-model potentials obtained for ^{7}Be+ ^{58}Ni, and the corresponding calculated reaction cross sections. The SPP is used for the real part V while the imaginary part is taken as $W = N_I \times V$.

E_{lab}	N_I	χ^2/N	σ_R (mb)
15.1	1.7	0.12	20.4±10
17.1	1.5	0.35	106±30
18.5	0.9	0.70	182±26
19.9	0.9	0.68	330±101
21.4	1.0	1.12	506±97

by the curves shown in Fig. 2. All χ^2/N values reported in this work refer to χ^2 per point. However, different parameters sets, with deeper real-well depths gave equivalent fits, these ambiguities are not relevant for the present work since the calculated total reaction cross section values were equivalent as long as the experimental angular distribution was properly fitted. It is worth pointing out that every acceptable potential had an imaginary part that extended beyond the corresponding real part. This suggests absorption at a large distance due to the existence of a halo state. The reaction cross sections are given in Table I.

For the ^{7}Be+^{58}Ni system, lower part in the Fig. 2, as was mentioned above, the inelastic scattering contribution to the quasi-elastic scattering was ignored in the optical model analysis. The Sao Paulo Potential (SPP) [41] was used for the real part of the Optical Potential, while the imaginary part was obtained by multiplying the real part times a factor N_I. This factor was chosen to fit the data for each energy, with the results shown in Table II. A good description of the data was obtained, as shown by the corresponding curves in the lower part of Fig. 2.

The evidence of halo effects can be seen when comparison of total reaction cross sections is made for different systems. In Fig. 3 the present results for ^{8}B and its core, ^{7}Be, are shown and compared with existing data for ^{6}He and its corresponding core ^{4}He [35, 36, 42, 43]. The data presented in this figure, were previously scaled by dividing the cross sections by the factor $(A_p^{1/3} + A_t^{1/3})^2$ and the energy by the factor $Z_p Z_t/(A_p^{1/3} + A_t^{1/3})$. Arguments have been given demonstrating that this procedure properly scales the normal geometrical and/or charge differences between systems without washing out the dynamical effects of interest [44]. It is clear from Fig. 3, that the reduced cross sections for the halo systems (^{8}B+^{58}Ni, ^{6}He+^{209}Bi, ^{6}He+^{64}Zn) look very similar and lie above those for the cores, *e.g.* ^{7}Be and ^{4}He respectively. The most interesting result is that the proton-halo nucleus ^{8}B data show an enhancement very similar to that present for the neutron-halo nucleus ^{6}He.

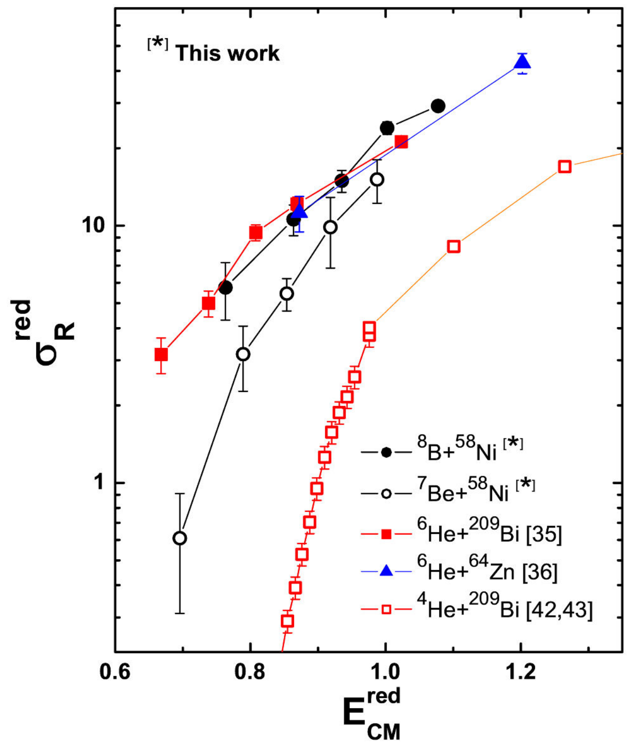

FIGURE 3. Reduced cross sections from the present work compared with other data. The curves are to guide the eye.

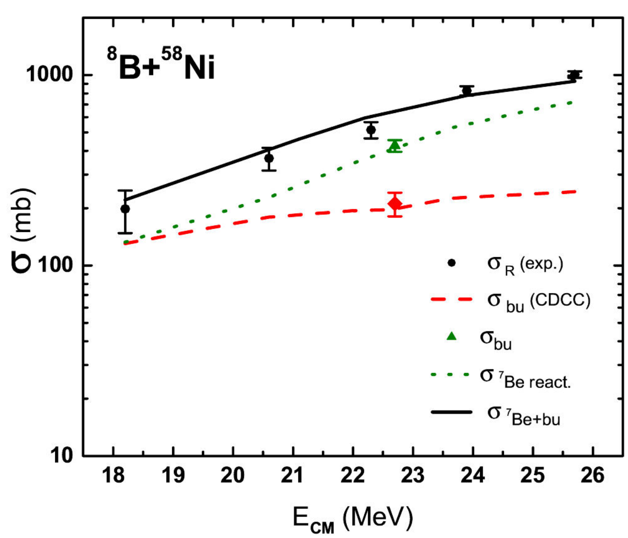

FIGURE 4. Total reaction and breakup cross sections for ^{8}B+^{58}Ni. The various curves that are discussed in the text.

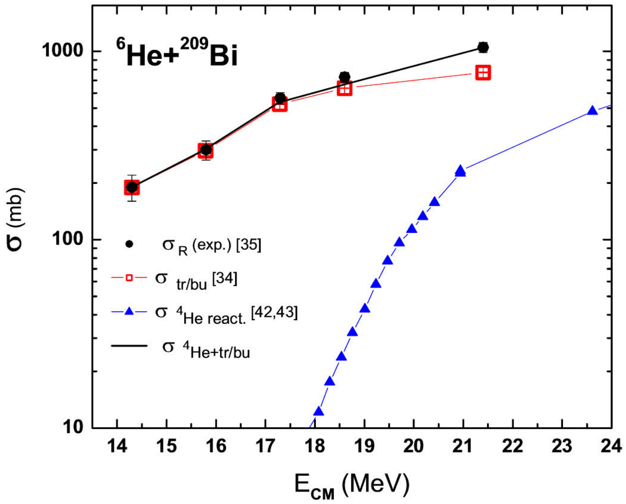

FIGURE 5. Total reaction and breakup/transfer cross sections for ^{6}He+^{209}Bi and total reaction cross sections for ^{4}He+^{209}Bi. The data were taken from Ref. 34,35,42,43.

The present work can give some insight into the role of transfer processes in the reactions of proton-halo systems. In this regard, it is interesting to compute the ^{8}B+^{58}Ni total reaction cross section from the ^{7}Be reduced reaction yield scaled according to the ^{8}B mass and charge, this is shown by the dotted curve in Fig. 4. The most important observation is that the sum of this curve plus the ^{8}B breakup yield from the CDCC calculation, dashed curve, reproduces the observed total reaction cross section almost perfectly (solid line in Fig. 4). In other words, the ^{8}B reaction cross section can be entirely accounted for by breakup of the halo state plus reactions that occur with the ^{7}Be core, leaving no room for proton transfer. This suggests an underlying decoupling between the core and the valence proton, which is an expected feature of a proton-halo state [11]. The present observations can then be taken as providing important evidence in favor of a proton-halo hypothesis for ^{8}B.

From Fig. 3, it could be expect that the total reaction cross sections for neutron-halo systems can be described under the same assumptions. For this purpose we considered the neutron-halo system ^{6}He+^{209}Bi. In Fig. 5 the previously reported total reaction and breakup/transfer cross sections for this system are presented [34,35]. The corresponding total reaction cross sections for the core, ^{4}He, on same target [42,43] also are displayed in this figure, properly scaled in the same way as for ^{8}B. It is clear from Fig. 5 that again the sum of breakup/transfer yield plus the total reaction cross sections of the ^{4}He, solid line, very well reproduce the total reaction cross sections of the neutron-halo ^{6}He leading to the same conclusion as for ^{8}B. Notice that in this case, the total reaction cross section for ^{6}He, is in fact saturated by the yield of breakup/transfer of the halo at lower energies.

In semiclassical terms, one would expect that in the case of ^{8}B, Coulomb polarization would result in the valence proton spending more time at large distances from the target, shielded by the core from the full Coulex effect. Core-halo breakup would occur mainly through the long range Coulomb force, and proton transfer would be suppressed. Esbensen and Bertsch [46] have shown that Coulomb breakup is in fact strongly modified by both the halo nature and the Coulomb polarization of the ^{8}B projectile. Despite this, the predicted breakup cross section is quite large in agreement with experiment. In the case of neutron-halo ^{6}He, Coulomb polarization favors neutrons in the halo residing in the region between the core and the target, which then enhances the reaction probabilities. Since these neutrons are closer to the target one can understand that they might tend to be transferred to it, consistent with observations for ^{6}He+^{209}Bi. In that system, most of the reaction yield comes from two-neutron transfer to neutron-unbound levels in the reaction product [45]. In contrast, an enhancement driven by particle transfer is not expected for a proton-halo system.

In summary, elastic-scattering angular distributions and total reaction cross sections for the (^{8}B, ^{7}Be) + ^{58}Ni systems are reported for energies around the Coulomb barrier. Comparison of reduced total reaction cross sections for ^{8}B with those reported for neutron-halo projectile ^{6}He, presents similar enhancementes for both projectiles. For both systems, it is shown that the sum of reaction yield of halo state plus total reaction cross section of the core very well describe the total reaction cross sections for ^{8}B and ^{6}He, suggesting a decoupling between the core and the nucleons forming the halo. It has been shown that a semiclassical ”picture” provides an explanation to understand the difference in the reaction process of halo nuclei. While the enhancement in the cross section observed for ^{8}B is explained in terms of projectile breakup, in the case of ^{6}He reactions, the particle transfer proces explains the observed enhancement.

Acknowledgments

This work has been partially supported by CONACYT, by FAPESP 2001/06676 and by the US NSF under Grant Nos. PHY06-52591 and PHY07-58100. E.F.A. acknowledges the hospitality of all personnel at the Notre Dame Nuclear Structure Laboratory.

1. T. Minamisono *et al.*, *Phys. Rev. Lett.* **69** (1992) 2058.
2. H. Kitagawa and H. Sagawa, *Phys. Lett. B* **299** (1993) 1.
3. H. Nakada and T. Otsuka, *Phys. Rev. C* **49** (1994) 886.
4. W. Schwab *et al.*, *Z. Phys. A* **350** (1995) 283.
5. R.E. Warner *et al.*, *Phys. Rev. C* **52** (1995) R1166.
6. I. Pecina *et al.*, *Phys. Rev. C* **52** (1995) 191.

7. F. Negoita *et al.*, *Phys. Rev. C* **54** (1996) 1787.
8. J.H. Kelley *et al.*, *Phys. Rev. Lett.* **77** (1996) 5020.
9. Y. Penionszhkevich, *Nucl.Phys. A* **616** (1997) 247c.
10. M.H. Smedberg *et al.*, *Phys. Lett. B* **452** (1999) 1.
11. S. Mizutori, J. Dobaczewski, G.A. Lalazissis, W. Nazarewicz, and P.G. Reinhard, *Phys. Rev. C* **61** (2000) 044326.
12. Y. Suzuki, R.G. Lovas, K. Yabana, and K. Varga, *Structure and reactions of light exotic nuclei*, Taylor& Francis, 2003.
13. V. Guimarães *et al.*, *Phys. Rev. Lett.* **84** (2000) 1862.
14. J. J. Kolata *et al.*, *Phys. Rev. C* **63** (2001) 024616.
15. H. Esbensen and G.F. Bertsch, *Phys. Rev. C* **59** (1999) 3240.
16. F.M. Nunes and I.J. Thompson, *Phys. Rev. C* **59** (1999) 2652.
17. J.A. Tostevin, F.M. Nunes, and I.J. Thompson, *Phys. Rev. C* **63** (2001) 024617.
18. E.F. Aguilera, E. Martinez-Quiroz, T.L. Belyaeva, J.J. Kolata and R. Leyte-Gonzalez, *Phys. At. Nucl.* **71** (2008) 1163.
19. L. Trache, F. Carstoiu, C.A. Gagliardi, and R.E. Tribble, *Phys. Rev. Lett.* **87** (2001) 271102.
20. D. Cortina-Gil *et al.*, *Phys. Lett. B* **529** (2002) 36.
21. D. Cortina-Gil *et al.*, *Nucl.Phys. A* **720** (2003) 3.
22. R.N. Majumdar, *J. Phys. Soc. Jpn.* **72** (2003) 3087.
23. M.S. Hussein *et al.*, *Phys. Lett. B* **640** (2006) 91.
24. T. Sumikama *et al.*, *Phys. Rev. C* **74** (2006) 024327.
25. C.A. Bertulani, *J. Phys. G: Nucl. Part.Phys.* **34** (2007) 315.
26. S. Karataglidis and K. Amos, *Phys. Lett. B* **650** (2007) 148.
27. L.F. Canto, P.R.S. Gomes, R. Donangelo, and M.S. Hussein, *Phys.Rep.* **424** (2006) 1.
28. N. Keeley, R. Raabe, N. Alamanos, and J.L. Sida, *Prog. Part. Nucl. Phys.* **59** (2007) 579.
29. Y.-J. Liang *et al.*; ArXiv 0708.0071 (2007). (http://adsabs.harvard.edu/abs/ 2007arXiv0708.0071L).
30. K.E. Rehm *et al.*, *Phys. Rev. Lett.* **81** (1998) 3341.
31. J.F. Liang *et al.*, *Phys. Lett. B* **491** (2000) 23.
32. A. Navin *et al.*, *Phys. Rev. Lett.* **81** (1998) 5089.
33. J.J. Kolata *et al.*, *Phys. Rev. Lett.* **81** (1998) 4580.
34. E.F. Aguilera *et al.*, *Phys. Rev. Lett.* **84** (2000) 5058.
35. E.F. Aguilera *et al.*, *Phys. Rev. C* **63** (2001) 061603(R).
36. A. DiPietro *et al.*, *Phys. Rev. C* **69** (2004) 044613.
37. A. Navin *et al.*, *Phys. Rev. C* **70** (2004) 044601.
38. E.F. Aguilera *et al.*, *Phys. Rev. C* **79** (2009) 021601(R).
39. M. Y. Lee *et al.*, *Nucl. Instr. Meth. A* **422** (1999) 536.
40. Z. Moroz *et al.*, *AIP Conference Proceedings* **69** (1981) 1102.
41. L.C. Chamon *et al.*, *Phys. Rev. C* **66** (2002) 014610.
42. A.R. Barnett and J.S. Lilley, *Phys. Rev. C* **9** (1974) 2010.
43. P. Sing *et al.*, *Phys. Rev. C* **43** (1991) 1867.
44. P.R.S. Gomes, J. Lubian, I. Padron, and R.M. Anjos, *Phys. Rev. C* **71** (2005) 017601.
45. P.A. DeYoung *et al.*, *Phys. Rev. C* **71** (2005) 051601(R).
46. H. Esbensen and G.F. Bertsch, *Phys. Rev. C* **66** (2002) 044609.